CFD Study on Aerosol Deposition in Human Upper Respiratory Tract

Kewu Zhu[1], Kwek Jin Wang[1], Tan RBH[12]

[1] Institute of Chemical and Engineering Sciences, 1, Pesek Road, Jurong Island,

Singapore 627833

[2] Department of Chemical & Molecular Engineering, National University of Singapore,

4 Engineering Drive 4, Singapore, 117576

Prepared for presentation at the 2004 AIChE Annual Meeting

Austin, Texas, November 7-12

Sept 2004

Unpublished

Abstract
Interest of aerosol deposition and transportation in airways of human lungs has increased in recent years with the efficient treatment of lung diseases, the exposure of people to airborne pollutants, and the potential for using inhaled aerosols as carriers of bio-therapeutics for systemic delivery. Flow dynamics and particle transportation at Upper Respiratory Tract (URT) will greatly influence aerosol transportation and deposition at deep lung airways. However, this aerosol deposition behavior is poorly understood. In this study, CFD simulations were carried out to investigate aerosol deposition patterns at an anatomically accurate (URT) geometry constructed using statistical data reported in the literature. Complicated laminar to turbulent transition flow dynamics at the URT was simulated using a k-ω turbulence model at various airflow rates. Investigation of transportation and deposition of aerosol particles was performed using a Lagrangian approach with one-way couple fluid-particle interaction. The present study revealed that inertial deposition is the dominant deposition mechanism at URT. Deposition and dispersion of particles with smaller STk number is strongly determined by local flow conditions. Results presented may be useful in guiding formulation of aerosol particle carriers for inhalation therapy.

1 Introduction

Interest in air flow and aerosol transport in airways of human being has increased in recent years with the efficient treatment of lung diseases, the risk associated with exposure of people to airborne pollutants, and the potential for using inhaled aerosols as carriers of bio-therapeutics for systemic delivery (Groberg, 2001; Wen *et al.*, 1996; Heenan *et al.*, 2003). Deposition of particles in the mouth is often overlooked in air pollution risk assessment due to its low particle deposition efficiency, and also because of complicated geometry variations arising from the movement of the tongue. In aerosol therapy, however, oral route, instead of nasal route, is often chosen as a drug delivery route to the lung taking advantage of its lower deposition efficiency. The understanding of particle deposition in the oral respiratory tract, however, is not yet complete due to its complicated geometry. Better understanding of the flow dynamics and the mechanisms of pulmonary particle deposition in the oral respiratory tract would be crucial to provide more effective treatments of lung diseases, better protect us from environmental airborne pollutants, and provide more effective routes of drug deliveries.

Many studies on air flow fields and aerosol deposition patterns in the lung and laryngeal region have been published in the literature (Hofmann and Koblinger, 1990; Edward, 1995), however, relatively few studies have been reported regarding aerosol particle deposition in the mouth and throat of human *Upper Respiratory Tract* (URT). Cheng *et al*. (1999) experimentally examined the effects of particle size (nine different size polystyrene latex fluorescent particles ranging from 0.93 to 30 μm) and breathing rate (three flow rates: 15, 30, 60 L/min) on the particle deposition patterns in a human oral airway replica. The oral cavity was molded from dental impression of an oral cavity in a human volunteer, while pharynx, larynx, trachea, and three generations of bronchi were made from cadaver. Their study revealed that deposition in the oral cavity increased with particle diameter and airflow rate. They also suggested that the minimum dimensions near larynx as well as the average cross-sectional area of the oral cavity were possible important parameters for an oral airway deposition. Corcoran and Chigier (2002) measured axial velocity and axial turbulence intensity patterns in the tracheal portion of a cadaver-based throat model at two different flow

conditions using Laser Doppler Velocimetry and qualitatively characterized aerosol deposition patterns using fluorescent dye. Heenan *et al.* (2003) measured air flow fields in an idealized human oropharynx using an endoscopic particle image velocimetry (PIV) at three flow rates: 15, 30, 60 L/min. Large deviations of numerical predictions for velocity profiles using a Reynolds-Averaged Navier-Stokes (RANS) CFD method from their PIV experimental measurements suggest more research work are necessary to elucidate the discrepancy and to improve the current numerical model.

Wen *et al.* (1996) investigated viscous stresses associated with airflows in 2D and 3D respiratory tracts using a 90^0 bend and a mouth-throat cast to model human oral-pharyngeal cavities respectively. Significant quantitative difference in viscous stress distribution was observed between a 90^0 bend model and an oropharyngeal geometry numerically reconstructed from a cast of human mouth and throat, which suggests the importance of a more physiologically faithful URT model. Kleinstreuer and Zhang (2003) analyzed the flow fields and particle deposition patterns using a particle tracking method with one-way fluid and particle coupling. The oral cavity/pharynx/larynx region was modeled as a near 180^0 curved bend with variable circular cross-sections of which the equivalent diameters were used the data reported by Cheng *et al.* (1999). Anatomically the cross section of pharynx is elliptical, pharynx airflow field is likely to be different and hence affects its particle dispersion and deposition patterns.

In the present study, an URT geometry having basic anatomical characteristic was constructed based on literature data reported by Fitch & Giedd (1999) and McRobbie et al. (2003). Knowing that pharynx deposition and dispersion is critical in the evaluation of DPI performance, elliptic cross section of pharynx representing the real anatomical structure was used in the URT model. CFD simulations of air flow and particle motion were carried out to investigate air flow field, particle deposition pattern and deposition mechanism at various air flow rates of interests to the application of dry powder inhalation therapy.

2. Geometry & mathematical model

Figure 1 shows the geometry used in the present work, which was constructed based on the literature data. Oral cavity, larynx, and trachea were modeled approximately as variable circular cross-sections of which diameters were calculated using the corresponding cross-sectional area measured by McRobbie *et al.* (2003) using MRI while the axial shape of URT was based on the study by Fitch & Giedd (1999). The pharynx was modeled as a cylinder with variable elliptical cross section of which the equivalent diameter was according to McRobbie *et al.* (2003).

Airflow in the constructed URT, modeled as an isothermal incompressible fluid, was solved using a CFD package Fluent 6. The model equations are:

$$\nabla \bullet \vec{u} = 0 \qquad (1)$$

$$\frac{\partial\left(\rho\vec{u}\right)}{\partial t}+\vec{u}\nabla\left(\rho\vec{u}\right)=-\nabla p+\left(\mu+\mu^{(t)}\right)\nabla^2\vec{u}+\rho g \qquad (2)$$

Where turbulent viscosity, $\mu^{(t)}$, is determined by

$$\mu^{(t)}=\alpha^*\frac{\rho k}{\omega} \qquad (3)$$

where, $\alpha^*=\left(0.024+\rho k/6\mu\omega\right)/\left(1+\rho k/6\mu\omega\right)$ (4)

Turbulent kinetic energy (k) and specific dissipation rate of turbulent kinetic energy (ω) can be solved using k-ω two equation models:

$$\frac{Dk}{Dt}=\frac{1}{\rho}\nabla\bullet\left[\left(\mu+\frac{\mu^{(t)}}{\sigma_k}\right)\nabla k\right]+\frac{1}{\rho}\bar{\bar{\tau}}:\nabla\vec{u}-\beta^*k\omega \qquad (5)$$

$$\frac{D\omega}{Dt}=\frac{1}{\rho}\nabla\bullet\left[\left(\mu+\frac{\mu^{(t)}}{\sigma_\omega}\right)\nabla\omega\right]+\frac{\alpha}{\mu^{(t)}}\bar{\bar{\tau}}:\nabla\vec{u}-\beta\omega^2 \qquad (6)$$

The parameters in the above model equations are δ_k= 2.0, δ_ω= 2.0, α=0.555, β=0.8333, β^*= 0.5

After obtaining airflow field, aerosol particles were released at zero velocity, representing breath activated DPI, from the inlet with uniform distribution over the cross section. Particles were considered to be deposited at the wall once it hits the wall. The number and initial positions of particle were input through a file generating using Matlab. Passively responding to the airflow field, trajectories of aerosol particles were computed according to Newtonian second law:

$$\frac{d\vec{s}}{dt}=\vec{v}\left(\vec{r},t\right) \qquad (7)$$

$$\frac{d\vec{v}}{dt}=\frac{\vec{u}-\vec{v}}{t_p}\frac{\mathrm{Re}_r C_D}{24}+\vec{g} \qquad (8)$$

$$\mathrm{Re}_r=\frac{\rho d_p\left|\vec{u}-\vec{v}\right|}{\mu} \qquad (9)$$

$$t_p=\frac{2}{9}\rho_p r_p^{\,2}/\mu * C_c \qquad (10)$$

$$C_c=1+\frac{2\lambda}{d_p}\left(1.257+0.4e^{-\left(1.1d_p/2\lambda\right)}\right) \qquad (11)$$

Instantaneous air velocity ($\vec{u}$) is composed of mean air velocity ($\bar{\vec{u}}$), obtained from equation (2), and fluctuation velocity ($\vec{u}'$). The local fluctuating velocities were obtained by multiplying the root-mean-square (RMS) air fluctuating velocity ($u_x' = u_y' = u_z' = (2k/3)^{0.5}$) by random numbers generated from a normal Gaussian probability density function at the start of every eddy-particle interaction. These random numbers are maintained constant during one eddy interaction.

3 Results and discussion

Simulations were carried out at different grid schemes to ensure numerical results having enough spatial resolution. Typical grid independent simulation results are shown in figure 2 where air flow profiles section 12 are presented at various grid resolutions. It was observed that difference in the prediction of airflow profiles between grid schemes (c) and (d) was negligible, and therefore prediction from grid scheme (d) can be considered as a grid independent result. Results presented in this report were all checked for grid independence as discussed above.

Figure 3 shows deposition efficiency as a function of impaction parameter, $d_{ae}^2 Q$. Where d_{ae} is aerosol aerodynamic diameter, and Q is the flow rate. Good agreements at larger impaction parameters were found between the numerical predictions and empirical correlations reported by Stahlhofen *et al.* (1989) and Cheng *et al.* (1999), although different geometries are used in these studies. This suggests that at URT inertial impaction is dominant deposition mechanism for larger impaction parameters. However, current model seems to over-predict the deposition efficiency at lower impaction parameters, suggesting local flow conditions might also influence the deposition efficiency, for example turbulence and secondary flow structure.

Figure 4 shows the vector plots of air and particle flow fields at section 6, one cross section at Pharynx cavity, at Re = 5500. Strong secondary flow structures – two distinct vortexes - were observed as a result of the curvature of the complicated URT geometry. Aerosol particles migrated to the peripheral of the vortex due to the centrifugal force and aerosol distribution depends on how well aerosol responds to the airflow field determined by the particle STk number. As one may notice that at smaller STk number particle follows airflow much closer, and its distribution exhibits more of the airflow features than particle with larger STk number, as shown in Figure 4.

Figure 5 presents aerosol deposition efficiency as a function of aerosol STk number. Compared to empirical correlation by Cheng et al. (1999), current model predicted the deposition efficiency quite well at larger STk number although different URT geometry was employed in the present work from those of Cheng et al. (1999) and Stahlhofen *et al.* (1989). Close agreements found between current model prediction and those experimental correlations at larger impaction parameter or STk number demonstrate that inertial impaction is the dominant deposition mechanism at the URT. However it was observed that current model over-predicted the deposition efficiency at smaller STk number. It seems that local flow condition has to be taken into account in the deposition efficiency prediction. For particles having larger STk number, it might be a good approximate to use STk based on its initial condition, as its behavior is inertia dominant. This is less true for particles with

smaller STk number as it follows the flow much closer. It might be more appropriate to use local STk number based on the local mean flow velocity (velocity scale) and local URT diameter (length scale). Figure 5-d shows the scatter plot of deposition efficiency as function of STk number based on local flow conditions. It was observed that predictions were substantially improved using the STk number based on local flow conditions.

4. Conclusions

In this study, geometry of human URT having basic anatomical features was constructed based on data reported in the literature. Simulations of airflow field and particle tracking were performed using the constructed geometry at airflow rates and particle sizes of interest to the application of dry powder inhalation therapy. It was found that secondary flow resulting from curvature of the URT has strong influence on the aerosol distribution depending on particle STk number. Higher deposition efficiency at higher Re and STk number suggests the deposition at URT be the inertial impact deposition dominant. Using STk number based on local flow condition, instead of flow at inlet, substantially improved the agreement between model predictions and empirical correlation experimentally determined at smaller STk number. This suggests that, comparing to larger aerosol particle, smaller aerosol particles response better to airflow and its deposition is likely to be more influenced by the local conditions. When evaluation of efficiency of dry powder inhalation therapy, in addition to the property of aerosol particles both geometry of respiratory tract and aerodynamics are very important.

References

Cheng, Y.S., Zhou, Y., Chen B. T. (1999) Particle deposition in a cast of human oral airways. *Aerosol Sci. and Technol.*, 31, 286-300.

Corcoran T.E. and Chigier N. (2002) A study of aerosol mechanics in the trachea using laser Doppler velocimetry and fluorescent dye. *ASME J. Biomechanical Eng.* 124(6), 629-637.

Edwards, D.A. (1995) The macrotransport theory of lung dispersion: aerosol deposition phenomena. *J. Aerosol Sci*. 26, 293-317.

Fitch, W. T. and Giedd J. (1999) Morphology and development of the human vocal tract: a study using magnetic resonance imaging. *J. Acoust Soc of America*, 106(3), 1511-1522.

Grotberg, J.B. (2001) Respiratory Fluid Mechanics and Transport processes. *Annu. Rev. Biomed. Eng.* 3, 421-457.

Heenan, A.F., Matida, E., Finlay, W. H. (2003) Experimental measurements and computational modeling of the flow field in an idealized human oropharynx. *Exp fluid*, 35, 70-84.

Hofmann, W. and Koblinger, L. (1990) Monte Carlo modeling of aerosol deposition in human lungs. Part II: deposition fractions and their sensitivity to parameter variations. *J. Aerosol Sci.* 21, 675-688.

Kleinstreuer, C., Zhang, Z. (2003) Laminar-to-turbulent fluid-particle flows in human airway model. *Int. J of multiphase flow*. 29, 271-289.

Mcrobbie D. W., Pritchard S, and Quest R. (2003) Studies of the human oropharyngeal airspaces using magnetic resonance imaging. I. Validation of a three dimensional MRI method for producing ex vivo virtual and physical casts of the Oropharyngeal airways during Inspiration. *J.Aerosol Med.*, 16 (4), 401-415..

Wen L. I., Perzl, M., Heyder, J., Langer, R., Brain, J.D., Englmeier K.H., Niven R. W., Edwards, D.A. (1996) Aerodynamics and aerosol particle deaggregation phenomena in model oral-pharyngeal cavities. *J Aerosol Sci.* 27(8), 1269-1286.

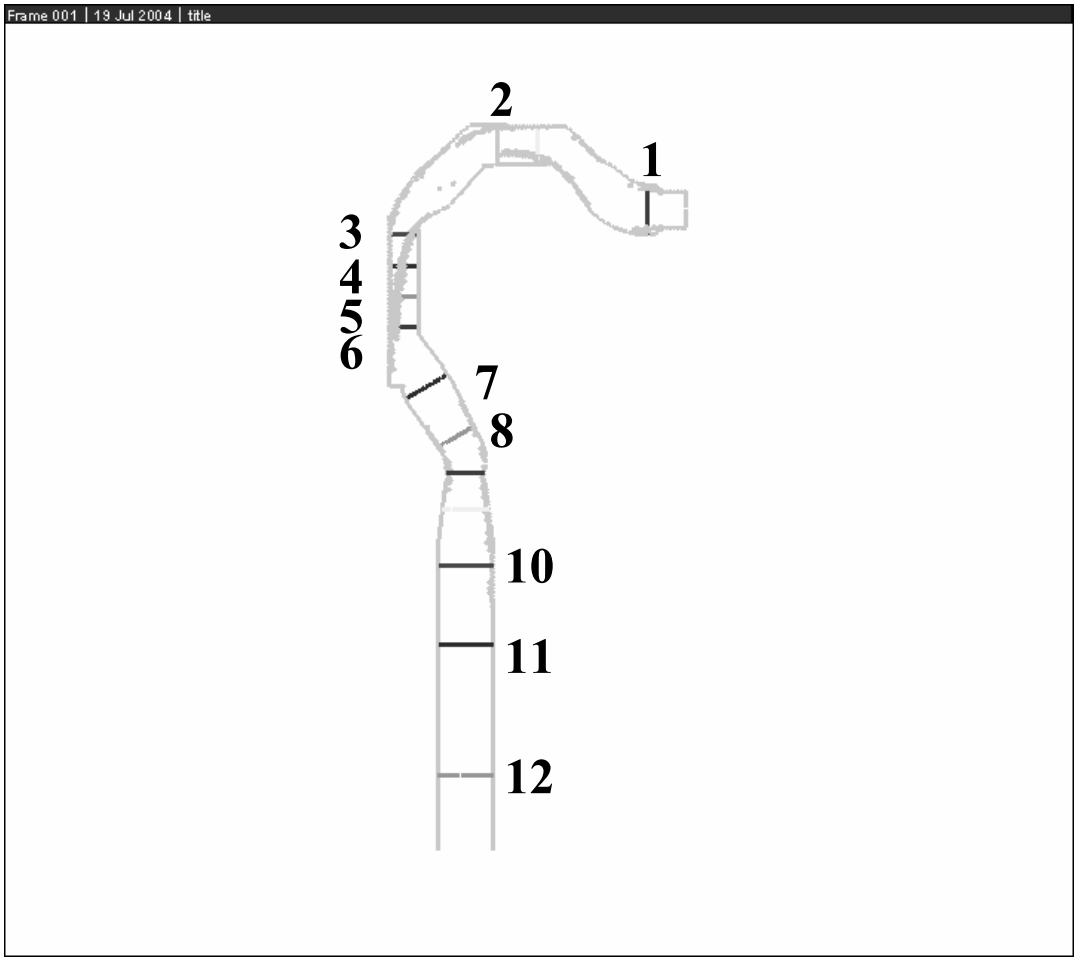

(a)

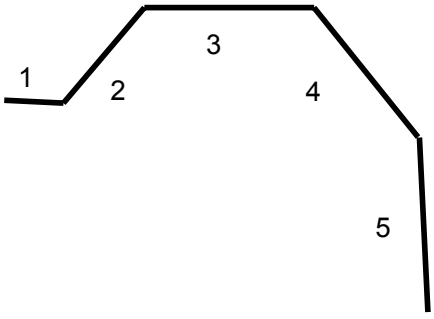

(b)

1:lip	**14.7mm**	**135^0**
2:blade	**23.5mm**	**139^0**
3:dorsum	**26.2mm**	**134^0**
4:velum	**33.7mm**	**139^0**
5:pharynx	**54.9mm**	

(c)

Figure 1: Schematic diagram human upper respiratory tract geometry (a); the axial length and relative position of oral cavity (b) &(c) .

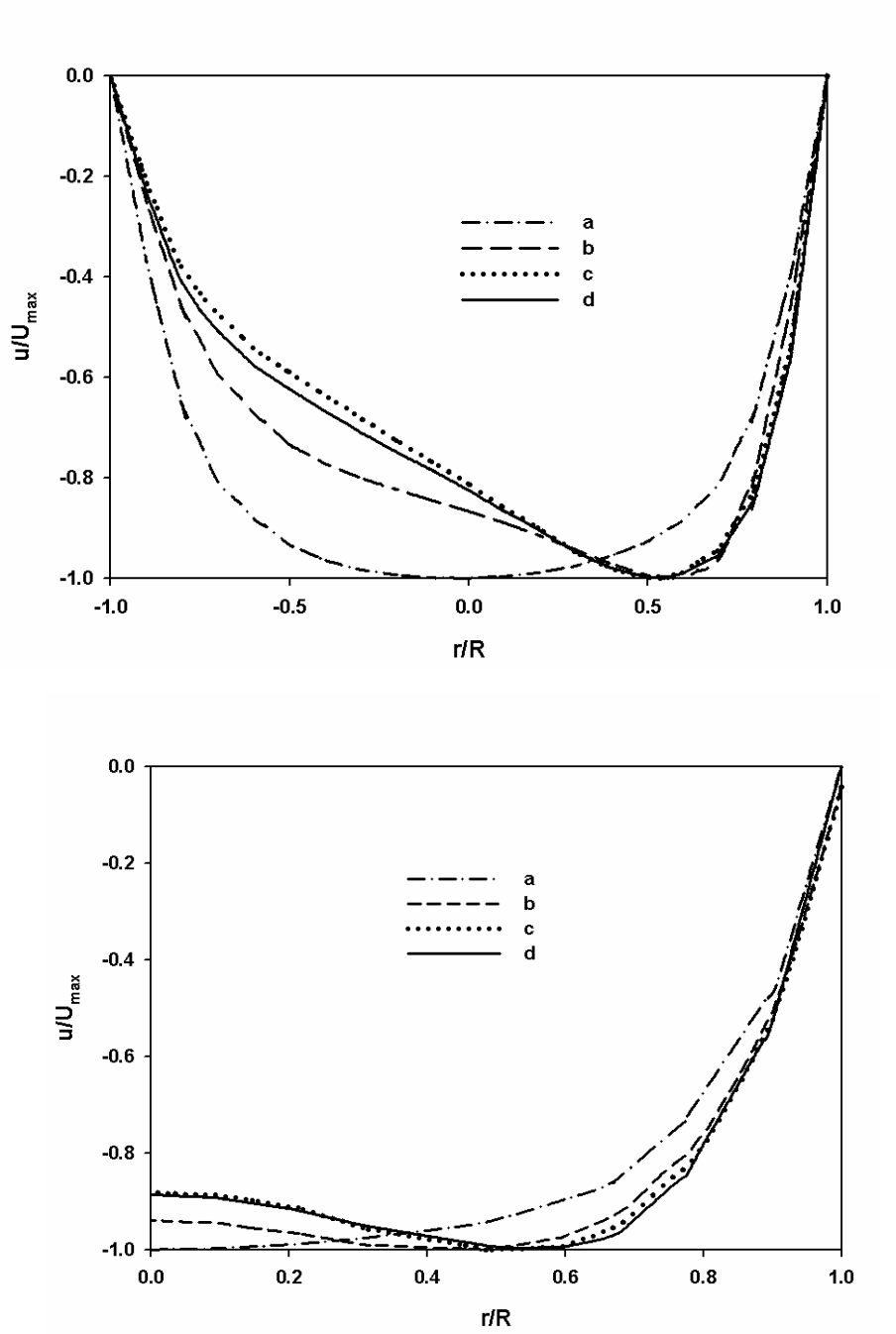

Figure 2: influence of grid schemes on air flow velocity at section 12 along the central line of, (a) back – front; (b) left – right. Re = 1900. (a) – 159127; (b) – 341459; (c) – 482271; (d) – 804738.

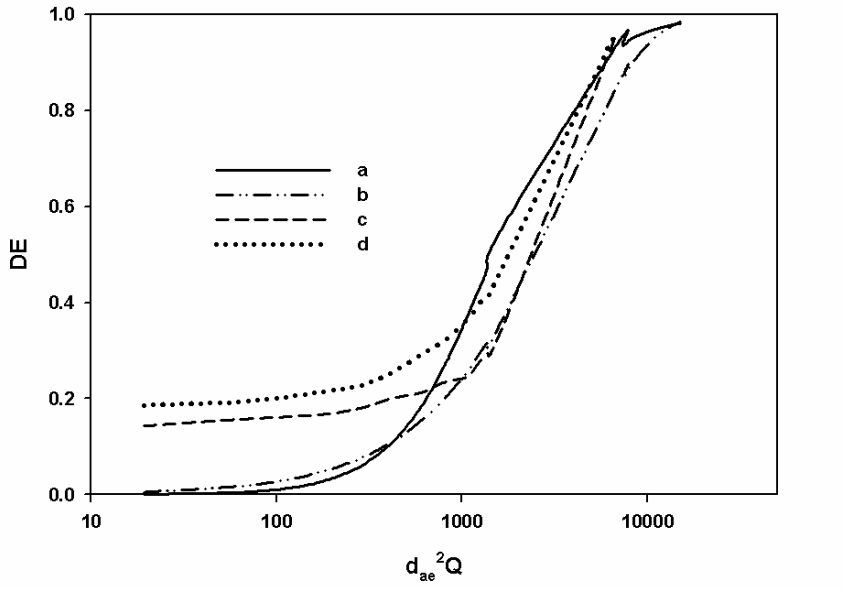

Figure 3: Plot of aerosol deposition efficiency with impaction parameter. (a) – Stahlhofen et al. 1989; (b) - Cheng et al. (1999); (c) – Mean flow tracking; (d) - Turbulent flow tracking

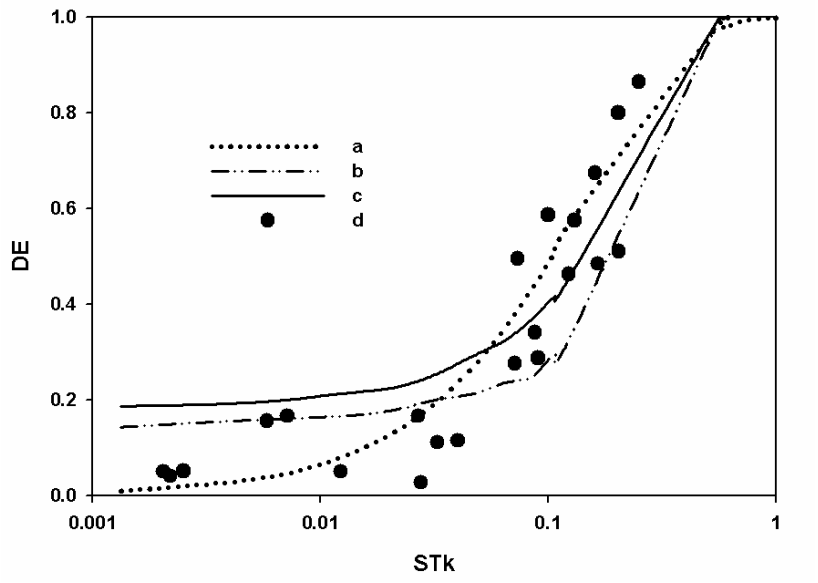

Figure 5: Plot of aerosol deposition efficiency with aerosol particle STk number. (a) – Cheng et al. (1999), STk number based on mean URT diameter; (b) – Mean flow tracking, STk number based on URT inlet diameter; (c) – turbulent flow tracking, STk based on URT inlet diameter; (d) – turbulent flow tracking, STk based on local URT diameter

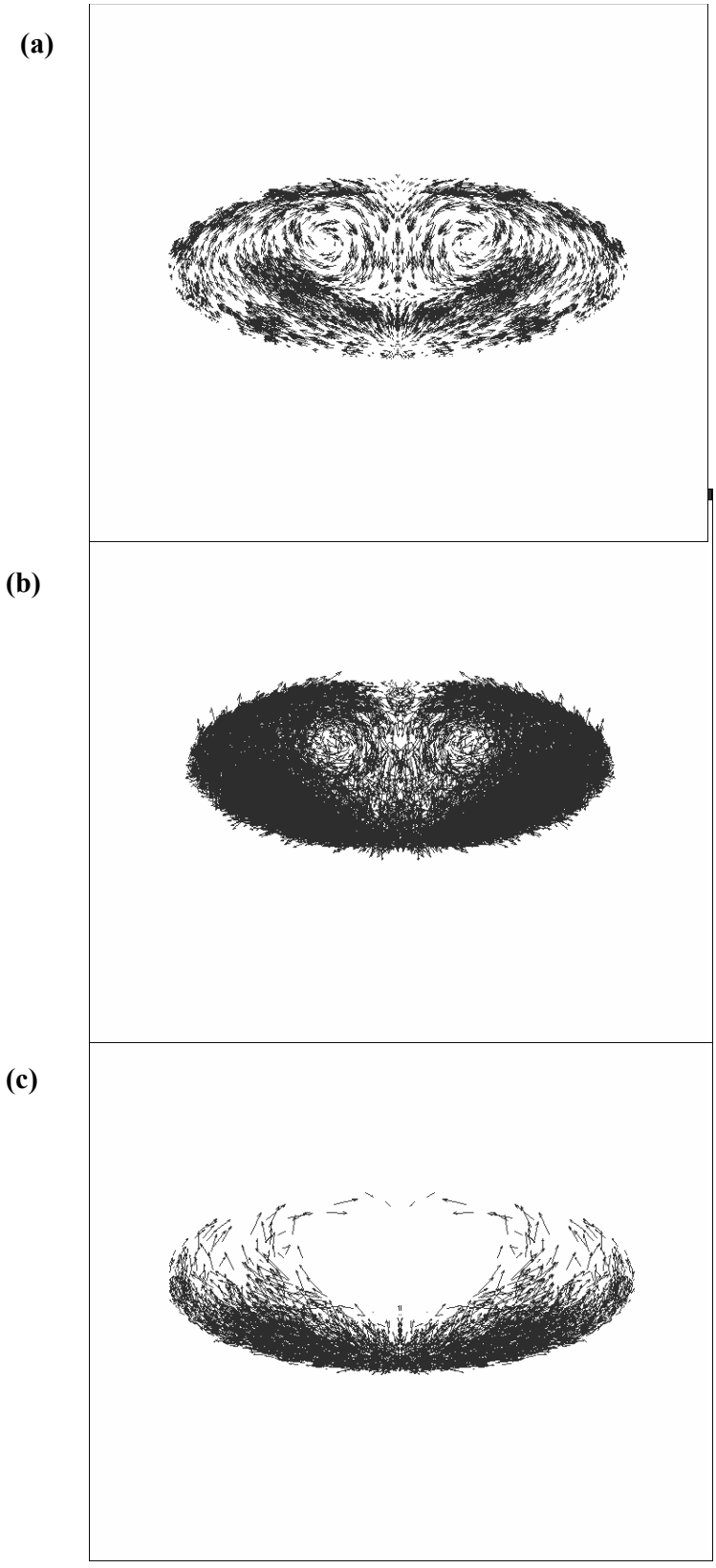

Figure 4: Vector plot of cross sectional distribution of aerosol particles at Re = 5500. (a) air secondary flow; (b) Stk = 0.005; (c) Stk = 0.08